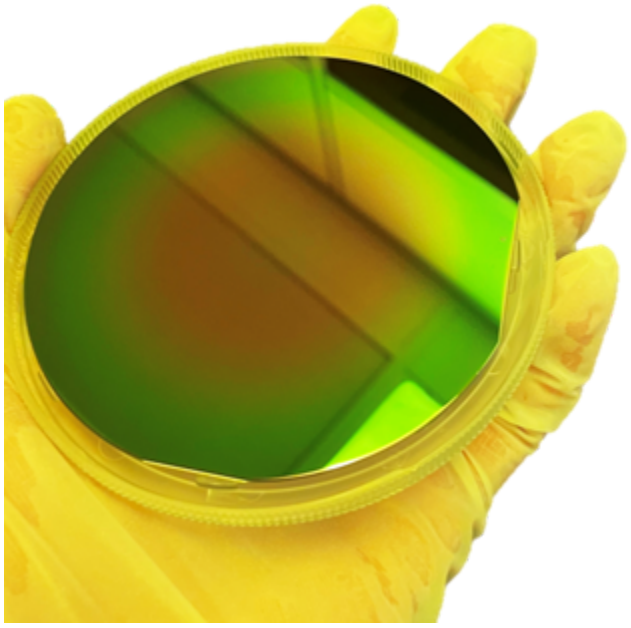

E241 Final Report:

MOCVD Growth and Nanofabrication of AlGaAs

Yan Joe Lee, Fenghao Xu, JP Berenguer

Spring 2022

Mentors: Jim Peterson, Mark Zdeblick, Archana Kumar

1. Acknowledgement

We would like to thank all E241 mentors and SNF staff for their invaluable advice and support throughout this project. In particular, we would like to thank our mentor Jim Peterson for his incredible helpfulness and expertise on everything MOCVD, our unofficial mentor Dr. Ben Reeves for his lessons on epitaxial growth of thin films and eagerness to guide us along every stage of the project, and Prof. Roger Howe for enthusiastically leading the course this quarter.

Part of this work was performed at the Stanford Nano Facilities (SNF). Part of this work was performed at the Stanford Nano Shared Facilities (SNSF), supported by the National Science Foundation under award ECCS-1542152.

2. Introduction

2.1. Motivation

The field of optics has historically relied on bulky optical elements to control and measure light. In the last couple decades, powered by advancements in simulation, fabrication, and characterization of nanostructures, the concept of metasurfaces emerged. These are subwavelength devices (fig. 1) that can be engineered to obtain arbitrary control over light absorption and emission functions [1]. Manipulating light at the nanoscale opens the door for several novel applications ranging from quantum communications to AR/VR displays.

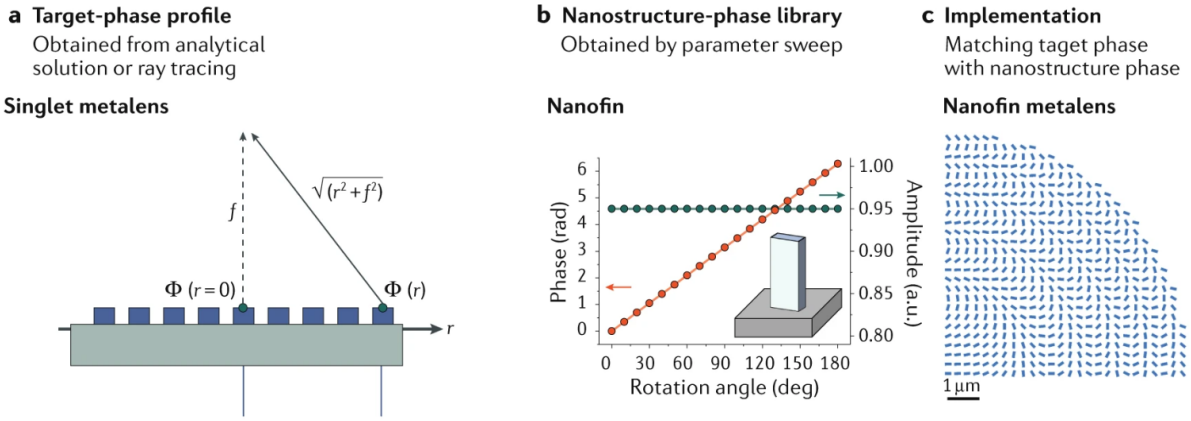

Figure 1: Step-by-step example of how to achieve arbitrary manipulation of wavefronts via metasurface design. First, we obtain a target-phase profile for each nanoblock in our metasurface to achieve the desired functionality, which in this case is to focus light at a focal point. Secondly, we sweep over a

geometrical parameter for our nanoblock to construct a nanostructure → phase library. Lastly, we match the target phase for each nanoblock with the specific geometry it requires. [2]

The ability of building blocks in all-dielectric metasurfaces to locally alter the optical phase front strongly depends on the metasurface/substrate index contrast. In addition, minimizing intrinsic optical losses is paramount to achieving high-efficiency metasurfaces. A potential candidate for such structures in the visible spectral range is $Al_xGa_{1-x}As$, a wide-bandgap semiconductor, which for high concentrations of aluminum ($x \simeq 0.8$) possesses high refractive index ($n = 3.56$) and very low extinction coefficient ($k = 7\times10^{-3}$) for $\lambda = 510$ nm. Also, AlGaAs is unique compared to other compound wide-bandgap semiconductors in that its lattice mismatch to the growth substrate (GaAs) is negligible (fig. 2), which greatly facilitates in-house epitaxial growth of thin films at SNF.

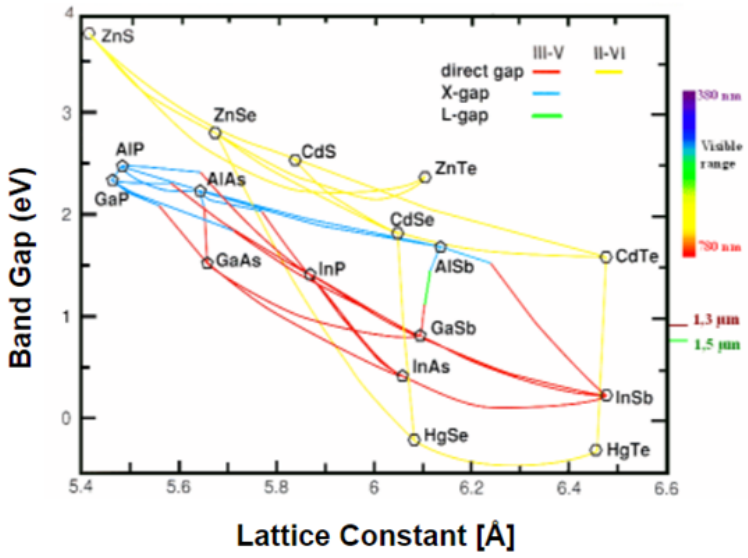

Figure 2: Diagram showing the bandgap and lattice constants for some of the most commonly used III-V and II-VI semiconductors.

2.2. Benefits to SNF and research community at Stanford

Our work is beneficial to SNF and the photonics research community at Stanford because it offers a guideline for growth and fabrication of high dielectric metasurfaces. In addition, it is the first study relating MOCVD III-V growth parameters to material composition, layer

thickness, and optical properties since the Aix200 long shutdown due to a major failure in 2021. We provide in this report useful guidelines for future users regarding MOCVD growth parameters, AlGaAs composition and refractive indices, E-beam lithography optimal doses, and plasma etching rates.

3. MOCVD

3.1. Overview

The tool used in this project for epitaxial III-V growth was the Aix200, a horizontal metalorganic chemical vapor deposition (MOCVD) system developed by Aixtron. The four main "knobs" to control growth parameters are: precursors' temperatures, chamber temperature, carrier gas flow, and precursor pressure. In the chamber, the wafer sits on a planetary satellite, which rotates via gas flow through its spiral channels in order to counteract the otherwise non-uniform deposition rates between upstream and downstream regions of the horizontal chamber (fig. 3)

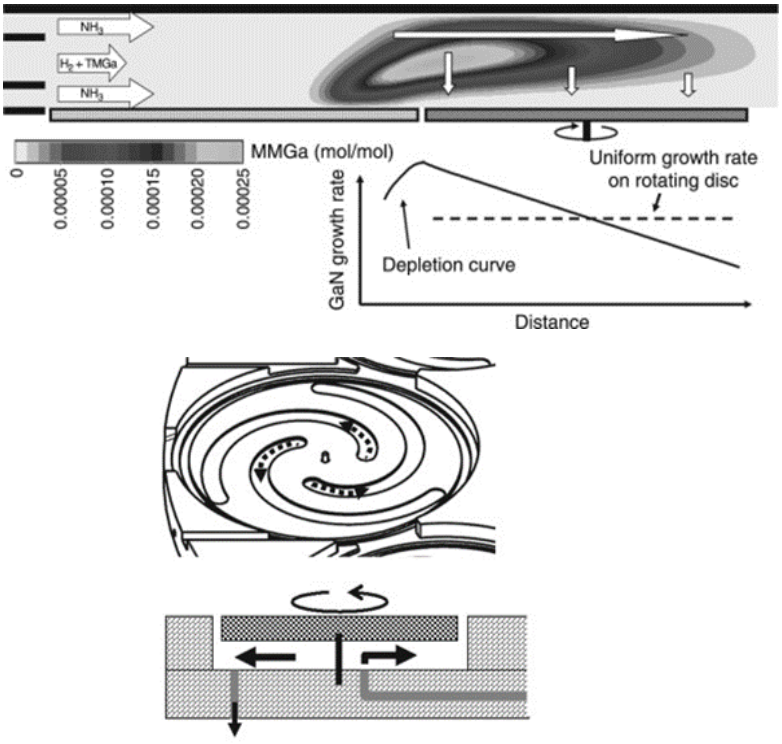

Figure 3: Schematic representation of a horizontal MOCVD chamber with a planetary satellite. The graph highlights the effect of a rotating wafer on leveling out the non-uniform deposition along the gas flow direction.

Before each growth, a "bakeout" recipe (BO775) was conducted, where the chamber temperature is raised to 775ºC under H_2 flow in order to remove possible contaminants previously deposited on the satellite. Then, a coating recipe was conducted where a thick (few microns) GaAs layer was grown on top of a dummy GaAs wafer in order to coat the chamber with the materials that would eventually be used in the growth.

The schematic structure of the grown film is depicted below (fig. 4) along with the targeted thickness/composition of each layer and their respective functions.

Figure 4: Schematic showing the recipe for growing our AlGaAs device layer (blue) in which we aim to pattern our metasurface. The various layers and substrate are labeled from 1-6 and their functions are described next to the schematic.

3.2. Preparation of recipe

In order to write the recipe to accurately achieve the targeted compositions and thicknesses, we utilized a custom-built spreadsheet that has been used by other groups at Stanford in the past to grow III-V films in the Aix200. We provided a separate guided tutorial as

a Nano Nugget on how to use the Excel spreadsheet to manipulate the tool parameters to achieve a targeted AlGaAs thickness and composition. In summary, there is empirical evidence from past users of the Aix200 that a 10 sccm molar flow of precursor TMGa at 5ºC for at 1500 mbar results in a 1.8 um/h growth rate of GaAs.

If we make the reasonable assumptions that the same growth rate applies to TMAl to grow AlAs; and that the ratio of the AlGaAs film composition will be the same as the ratio of TMAl and TMGa molar flow, we can extrapolate the empirical data point for GaAs in order to obtain growth times for AlGaAs and AlAs as well. The text file with the detailed commented code used for the recipe can be retrieved in the Aix200 system and we also provided it as a Nano Nugget. There, one can find specific parameters we chose regarding source pressures, temperatures, methods to ensure carrier gas flow stabilization, As overpressure, etc.

3.3. 1st growth campaign

The first growth was partially successful. On the one hand, we obtained crystalline film growth with reasonable composition accuracy, as evidenced by comparing the optical constants to literature values (fig. 5), which might not have been the case given the complex maintenance job the tool had to undergo for months.

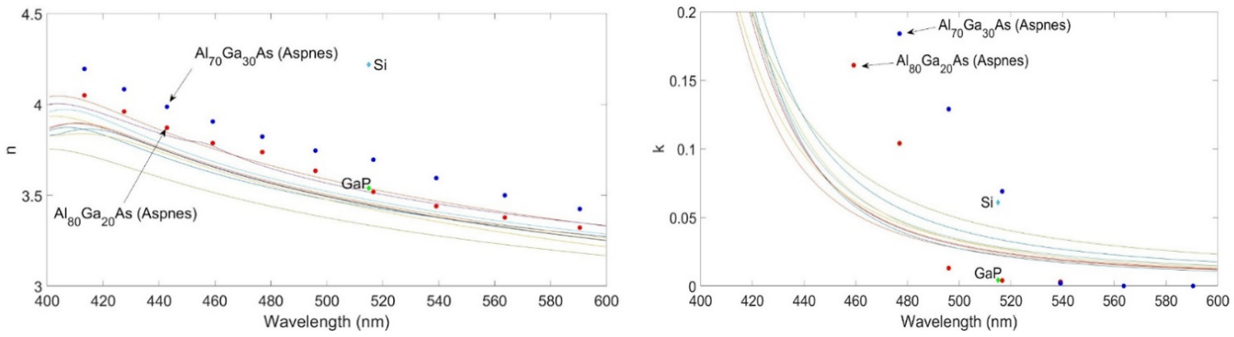

Figure 5: The differently colored curves show the spectral-dependence of the refractive index that was measured on different locations of the grown films. The top panel shows the spectra for the real part of the refractive index and bottom panel shows the corresponding spectra for the imaginary part of the refractive index.

On the other hand, the deposition rates were highly non-uniform leading to extreme variations in thicknesses across the wafer (fig. 6). The observed interference patterns were symmetric along the gas flow direction, which indicated there was an issue with the satellite rotation. After troubleshooting sessions, we concluded the installed satellite was incompatible with the current chamber conditions and does not rotate properly. A different satellite was installed and tested to ensure proper rotation. Then, it underwent bake out and coating runs in preparation for the 2nd growth.

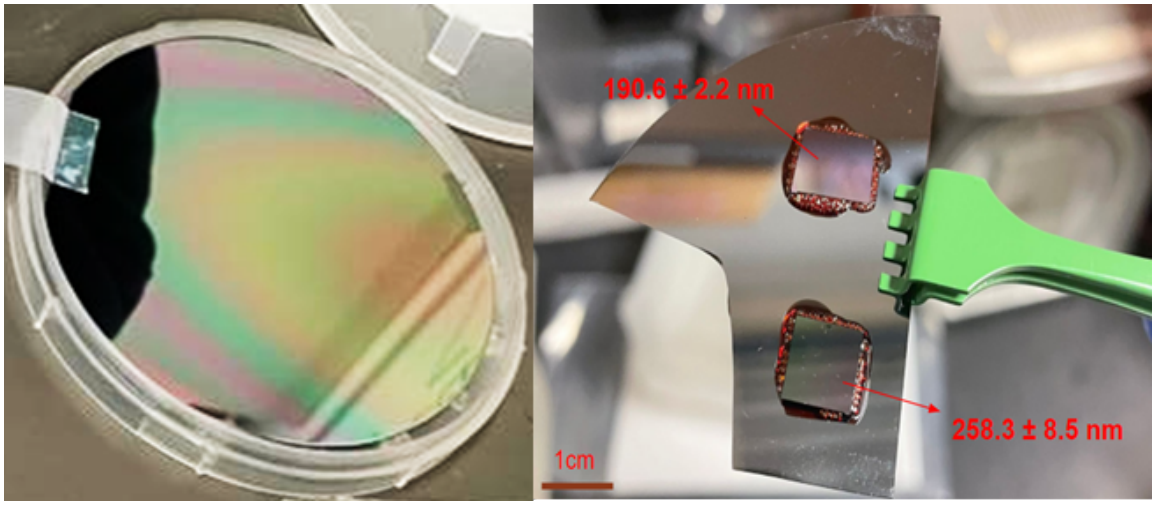

Figure 6: Photograph of the grown wafer (left) and selected areas that we analyzed with ellipsometry to measure the optical properties and refractive index.

3.4. 2nd growth campaign

A new satellite was installed in the MOCVD chamber and the second growth campaign showed significant improvements (fig. 7). Firstly, the radially symmetric interference patterns indicate that the rotational issue was resolved. Most importantly, the thickness variation was greatly reduced; ellipsometry measurements indicate an average AlGaAs layer thickness of 275nm with a wafer scale uniformity of 7%. Since the metasurfaces will eventually be patterned on a very small region compared to the entire wafer, we can continue to the next stage of the project, which involves e-beam lithography, metal evaporation, and plasma etching.

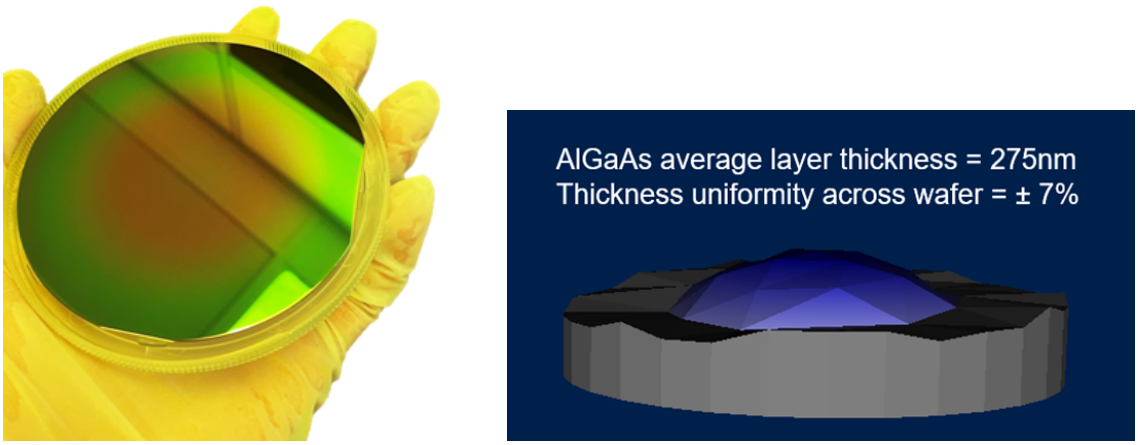

Figure 7: Photograph of a wafer with a more uniformly-grown AlGaAs layer (left) and 3D rendering of AlGaAs layer thickness obtained via ellipsometry on a wafer scale.

3.5. Additional remarks

There are two important final remarks to be made that can be helpful to future Aix200 users. Firstly, even though we achieved an acceptable wafer-scale deposition rate uniformity for our application (metasurfaces), a potential way to reduce thickness variation even more would be to reduce the satellite rotation. The satellite in this tool is not motorized; it instead relies on gas flow (underneath the wafer) through its spiral channels to rotate. If this gas flow is too large, it will carry heat away from the wafer via convection too quickly and affect the deposition rate uniformity. The radially symmetric interference patterns strongly suggest this occurred in our 2nd growth; thus, future users may use our rotational gas flow value as the reference for a maximum value when growing GaAs, AlAs, AlGaAs. Secondly, we saw a consistent overshooting in layer thickness for all of our layers of about 1.3X compared to the target thickness. For the purpose of fabricating metasurfaces, this is not an issue as the device layer can be dry etched later. For future users that may need better accuracy, we recommend a correction on the growth times calculated by the spreadsheet, as detailed in the Nano Nugget, though we cannot specify the correction quotient since our thickness measurements were only obtained indirectly through ellipsometry/reflectometry.

4. Nanofabrication

4.1. Overview

To fabricate high-refractive-index AlGaAs metasurfaces on low-index substrate, we proposed three different methods that can isolate the AlGaAs layer from growth substrates and nano-pattern and bond onto a quartz supporting substrate. The first method starts with an indirect bonding from as-grown AlGaAs pieces onto the quartz substrate, and then uses selective wet etching to isolate the AlGaAs layer on which a metasurface is patterned. This process requests an optical low-loss adhesive that can handle high temperature for nanofabrication, and is chemically resistant to solvents and wet etchants.

The second method instead starts directly nanopatterning AlGaAs layers on the growth substrate. Once the metasurface is defined, a layer of spincoated HSQ fills and insulates AlGaAs elements for planzaitzation. Then the sample is bonded on quartz, followed by selective wet etching to remove the growth substrate. Finally the metasurface is encapsulated by another HSQ layer. One advantage for this method is that the adhesive layer is spatially separated from the metasurface, which reduces light scattering and absorption adjacent to the metasurfaces. Also we could avoid possible development/lift-off failures in the e-beam lithography process due to the existing adhesive layer, which is typically less chemically resistant and not low enough coefficient of thermal expansion.

The third method would be ideal if we could achieve a direct bonding in SNF. The AlGaAs and handling layers are first isolated by selective wet etching. Then in principle, the AlGaAs layer can directly bond onto quartz, given a perfect van de Waals bonding at the interface. However, there is no direct bonding machine with pre-plasma surface treatment in SNF. An imperfect bonding might lose the contact of AlGaAs layers in the lithography process.

For the class project, we chose the 2nd method that allowed us to go through the lithography and etching by using standard machines in SNF/SNSF facilities. The following sessions are our progress on nano-patterning AlGaAs on the growth substrates. In the long term we would also like to update our results on selective etching and bonding.

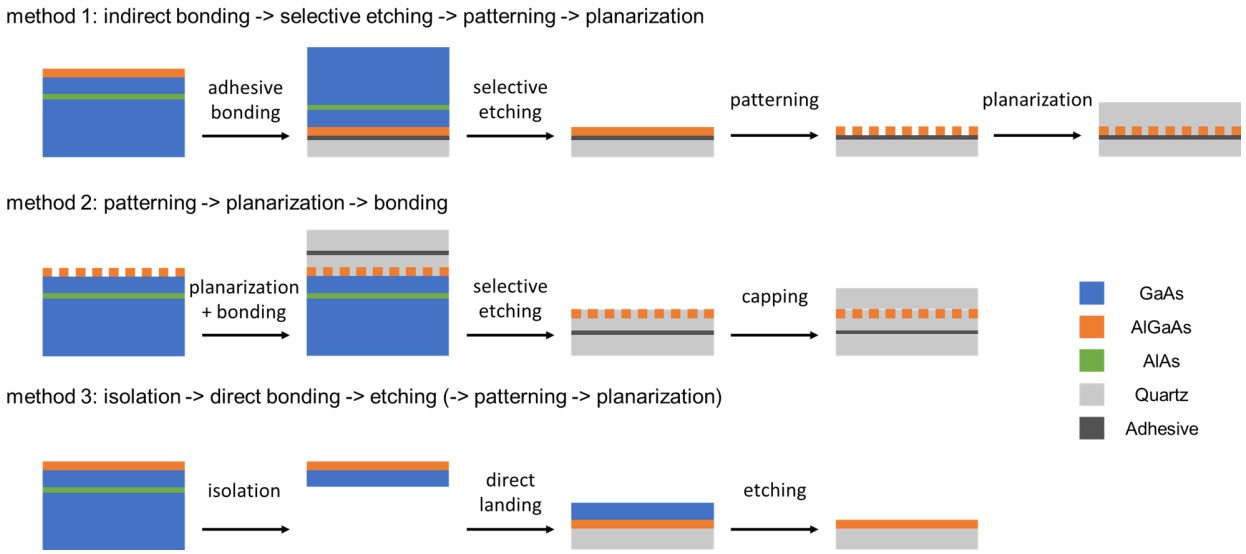

Figure 8: Potential methods to achieve nano-patterning and transferring AlGaAs layers on low index substrates.

4.2. Electron beam lithography process

The e-beam lithography process used to pattern the nanostructure is outlined in the schematic below.

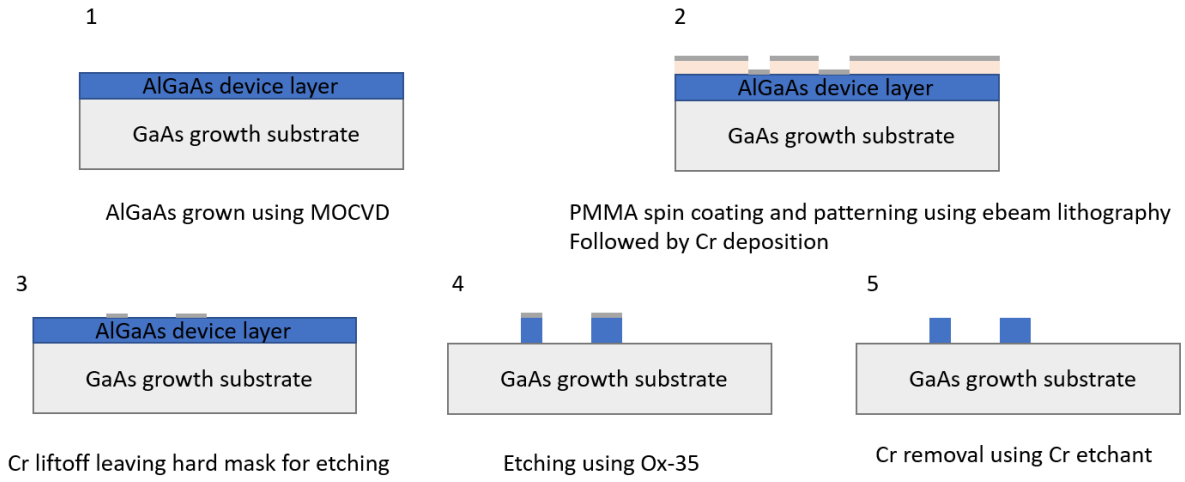

Figure 9: E-beam lithography and deposition schematic for patterning nanostructures.

We first chose to use a double layer MMA-PMMA e-beam resist process for the lithography in order to achieve an undercut lift-off profile. We used the Raith Voyager Electron

Beam Lithography system in the SNSF for the nanopatterning. The unit cell for our periodic structure consists of two nanobeams of 48 nm and 120 nm widths, spaced 145 nm apart. To determine the optimal e-beam dose, we performed a dose test using the smallest beam current which is 1 nA to achieve a high resolution for our sub-100 nm structures. We determined that a dose of around 300 $\mu C/cm^2$ is ideal for our structures. The resulting optical images of the e-beam resist after patterning and development are shown below.

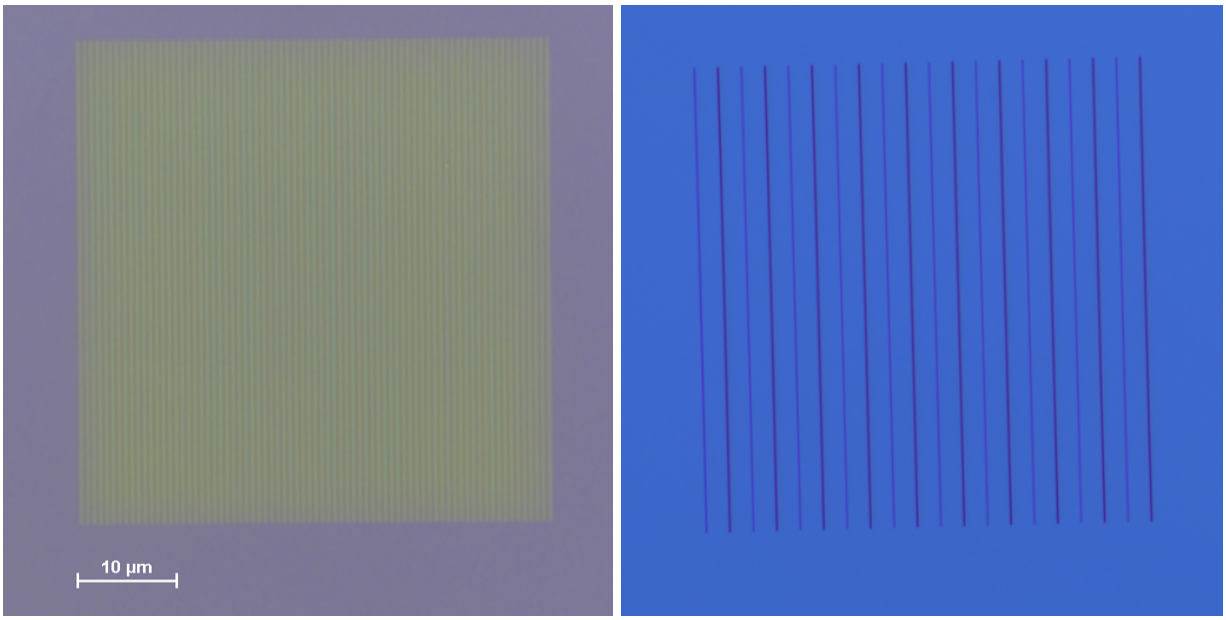

Figure 10: E-beam resist after development for periodic structures in final metasurface design (left) and constituent nanobeams in unit cell spaced out (right)

4.3. Evaporation

In order to pattern the AlGaAs layer into the desired nanostructures, we decided to use Cr as a hard mask for etching. To deposit the Cr layer, we used the KJL e-beam evaporator in the SNSF with the standard 3 A/s recipe. We started with a 50 nm layer, but the Cr etches at a considerable rate (although still significantly slower than AlGaAs) as elaborated in the plasma etching section below. Hence further investigation is needed for an adequate Cr etch mask thickness. This is also limited by the e-beam resist recipe since the Cr mask thickness has to be less than the resist thickness for the lift-off process to work.

4.4. Plasma etching

Dry etching our samples via Inductive Coupled Plasma Reactive Ion Etching (ICP-RIE) proved to be more complex than anticipated; thus, our results are still rather preliminary. We first attempted to follow a recipe listed in the tool's (Ox-35) standard operating procedure, recipe name: AR- GaAs Etch (High eR) - BCl3/Cl2, which had a reported GaAs etch rate of 2.16 nm/s. However, our ellipsometry results suggested an etch rate of almost 10x the reported value. In addition, because the available recipes had very high etch rates and our AlGaAs device film was only ~270 nm, we attempted to etch many samples for tens of seconds, resulting in inconsistent and non-linear etch rates, which we hypothesize it comes from the instability in the chamber conditions during the beginning of the etch. That is, it takes more than 10s for the capacitor/plasma properties to stabilize, as evidenced by the tool monitor.

We then created a recipe based on a paper by Agarwala et al. [3] where a thorough mixture design experiment was conducted to obtain etch rates as a function of Cl_2, BCl_3, and Ar partial pressures. This allowed us to target much lower etch rates and, thus, longer etch times which give enough time for the ICP-RIE to reach a steady-state. Unfortunately, the NOVA SEM was shut down during the week we conducted these experiments, so we could not obtain SEM images of the etching process and only had indirect results from reflectometry. Below (fig. 9) is an example of an etch rate we obtained that was fairly close to the one predicted by the ref. [3].

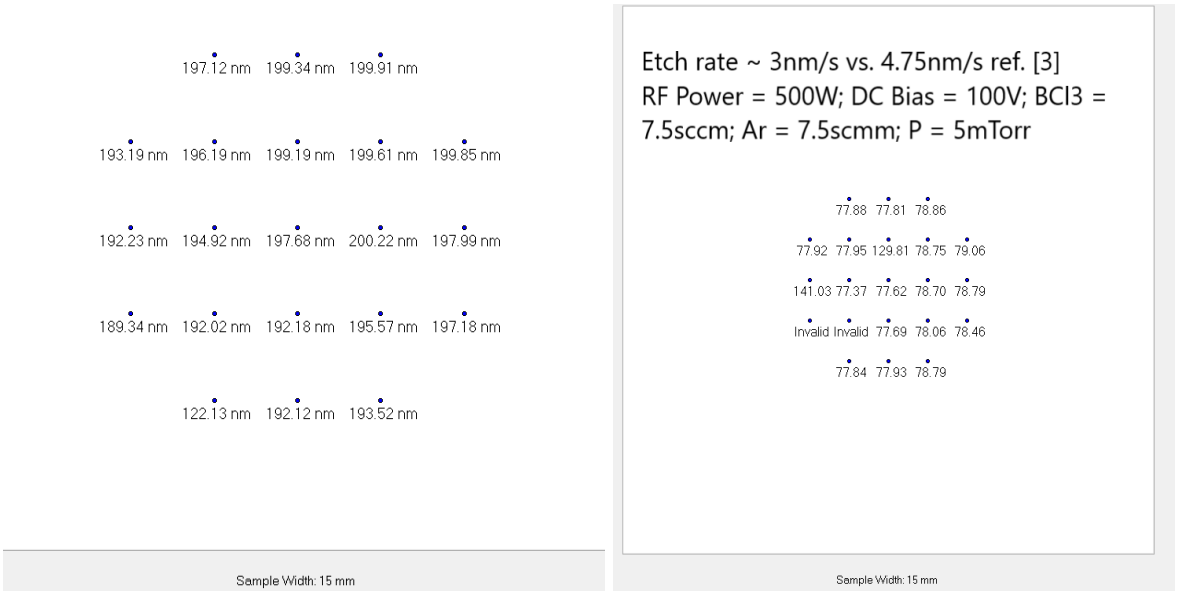

Figure 9: Schematic map obtained by reflectometry depicting the AlGaAs layer thickness in different regions of a 1.5cm x 1.5cm sample. The recipe used is provided as well as a comparison to the literature values in ref. [3].

Although we could not access the SEM, we conducted Atomic Force Microscopy (AFM) measurements on a nanopatterned sample that underwent plasma etching. The 3D profiles below (fig. 10) gives us a good indication that Cr also etches at a considerable rate for the recipes chosen, since the heights of our nanobeams were much lower than expected; thus we will work on optimizing the thickness of our masks in future lithography runs. In addition, the attempted pattern only contained two beams per unit cell, thus the lack of a clear valley between the beams suggests a non-successful liftoff process or e-beam exposure.

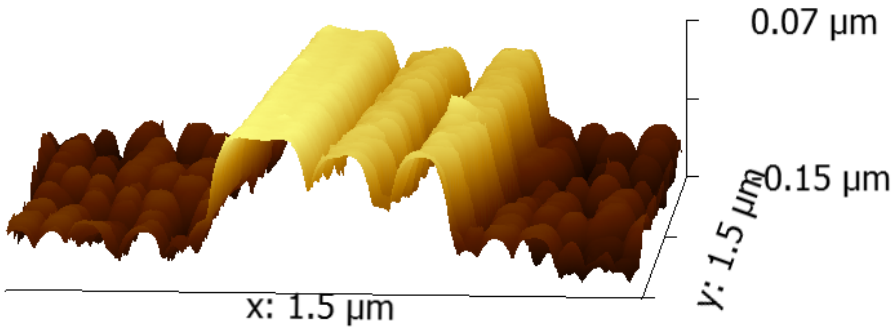

Figure 10: AFM images of patterned unit cell containing two nanobeams.

5. Conclusion

In our project, we explored two directions. First, we successfully demonstrated epitaxial growth of GaAs, AlAs, and AlGaAs layers with reasonable thickness and composition accuracy. The specific recipe we used is available on the tool for any future Aix200 user and we provided a guided tutorial (Nano Nugget) on how to adjust the tool's parameters to target a specific AlGaAs composition and growth rate. Second, we made significant progress on the nanofabrication of

AlGaAs metasurfaces and shared the details of successes and failures along the journey that may be helpful to future photonics research on high dielectric nanostructures. We provided quantitative and qualitative reports on our results in various stages of spin coating, e-beam lithography, metal evaporation, and plasma etching.

6. Future Work

We plan on providing updates on our future endeavors on this project for the benefit of SNF users and the Stanford photonics community at large. In an eventual 3rd growth campaign, we will make adjustments to our recipe (as previously discussed) in order to improve the deposition rate non-uniformity even further. Regarding the nanofabrication of metasurfaces, we will work on optimizing a single-layer resist recipe and obtaining plasma etching recipes with reproducible etch rates, which will be easier to characterize when the Nova SEM is fully functional again. Finally, we will develop a method to bond AlGaAs nanostructures to low-index substrates for high-efficiency metasurfaces.

7. Budget

		Members	Rate	Subtotal	Comments
Training	aix200	3	$400	$1,200	
	Ox-35	3	$95	$285	
		Hours	**Rate(/h)**	**Subtotal**	
Tool time	wafersaw	1h45min	$35	$96.25	
	woollam	3h38min	$50	$181.67	
	Ox-35	7h29min	$50	$374.17	
	xactix	22min	$50	$18.33	
	KJL	58min	$35	$33.83	
	XE-70	2h30min	$20	$50.00	
	aix200	9h4min	$100	$906.67	1st growth
	aix200	12h14min	$100	$1263.33	2nd growth
	Name	**Counts**	**Price**	**Subtotal**	
Supplies	GaAs 4” Wafers	5	$220	$1,100	from group expense, not included
	Au (KJL)	60nm	$1.177	$70.64	
		Grand Total		$4479.89	

8. References

[1] Brongersma, Mark L. "The road to atomically thin metasurface optics." *Nanophotonics* 10.1 (2021): 643-654.

[2] Chen, Wei Ting, Alexander Y. Zhu, and Federico Capasso. "Flat optics with dispersion-engineered metasurfaces." *Nature Reviews Materials* 5.8 (2020): 604-620.

[3] Agarwala, Sambhu, et al. "High-density inductively coupled plasma etching of GaAs/AlGaAs in BCl 3/Cl 2/Ar: A study using a mixture design experiment." *Journal of Vacuum Science & Technology B: Microelectronics and Nanometer Structures Processing, Measurement, and Phenomena* 16.2 (1998): 511-514.